HAL
open science

Microstructural evolution in Al-Mn-Cu-(Be) alloys

Niko Rozman, Jozef Medved, Franc Zupanic

To cite this version:

Niko Rozman, Jozef Medved, Franc Zupanic. Microstructural evolution in Al-Mn-Cu-(Be) alloys. Philosophical Magazine, 2011, pp.1. 10.1080/14786435.2011.608733 . hal-00728899

HAL Id: hal-00728899

https://hal.science/hal-00728899v1

Submitted on 7 Sep 2012

HAL is a multi-disciplinary open access archive for the deposit and dissemination of scientific research documents, whether they are published or not. The documents may come from teaching and research institutions in France or abroad, or from public or private research centers.

L'archive ouverte pluridisciplinaire **HAL**, est destinée au dépôt et à la diffusion de documents scientifiques de niveau recherche, publiés ou non, émanant des établissements d'enseignement et de recherche français ou étrangers, des laboratoires publics ou privés.

Microstructural evolution in Al-Mn-Cu-(Be) alloys

Journal:	*Philosophical Magazine & Philosophical Magazine Letters*
Manuscript ID:	TPHM-11-Apr-0154.R1
Journal Selection:	Philosophical Magazine
Date Submitted by the Author:	16-Jul-2011
Complete List of Authors:	Rozman, Niko; University of Maribor, Faculty of Mechanical Engineering Medved, Jozef; University of Ljubljana, Faculty of Natural Sciences and Engineering Zupanic, Franc; University of Maribor, Faculty of Mechanical Engineering
Keywords:	aluminium alloys, quasicrystalline alloys, microstructure, microhardness
Keywords (user supplied):	

SCHOLARONE™
Manuscripts

Microstructural evolution in Al-Mn-Cu-(Be) alloys

Niko Rozman[1], Jožef Medved[2], Franc Zupanič[1]

University of Maribor, Faculty of mechanical engineering, Maribor, Slovenia

University in Ljubljana, Faculty of Natural Sciences and Engineering, Slovenia

Corresponding author
Franc Zupanič
University of Maribor
Faculty of Mechanical Engineering
Smetanova 17
SI-2000 Maribor
Slovenia
tel. +386 2 220 7863
fax. +386 2 220 7990
e-mail: franc.zupanic@uni-mb.si

.

For Peer Review Only

Microstructural evolution in Al-Mn-Cu-(Be) alloys

This article investigates the effects of alloying elements on the microstructural evolution of Al-rich Al-Mn-Cu-(Be) alloys during solidification, and subsequent heating and annealing. The samples were characterized using scanning electron microscopy, energy dispersive X-ray spectroscopy, synchrotron X-ray diffraction, time-of-flight secondary-ion mass spectroscopy, and differential scanning calorimetry. In the ternary $Al_{94}Mn_3Cu_3$ (at. %) alloy, the phases formed during slower cooling (≈ 1 K s^{-1}) can be predicted by the known Al-Mn-Cu phase diagram. The addition of Be prevented the formation of Al_6Mn, decreased the fraction of τ_1-$Al_{29}Mn_6Cu_4$, and increased the fraction of Al_4Mn. During faster cooling (≈ 1000 K s^{-1}), Al_4Mn predominantly formed in the ternary alloy, whereas in the quaternary alloys the icosahedral quasicrystalline phase dominated. Further heating and annealing of the alloys caused an increase in the volume fractions of τ_1 in all alloys, and $Be_4Al(Mn,Cu)$ in quaternary alloys, while fractions of all other intermetallic phases decreased. Solidification with a moderate cooling rate (≈1000 K s^{-1}) caused considerable strengthening, which was reduced by annealing for up to 25 % in the quaternary alloys, while hardness remained almost the same in the ternary alloy.

Keywords: aluminium; quasicrystal; microstructure; beryllium

1 Introduction

Modern engineering materials must be able to carry high load and simultaneously possess high reliability. The materials of choice have high-strength, high-toughness, and low density. From among them, aluminium alloys still play an important role, in spite of the rapid development of lighter magnesium alloys and different types of lightweight composites. Al-casting alloys have been used successfully in many applications in the automotive and aerospace industries. The most versatile Al-Si alloys can attain a very wide range of properties, the strongest ones e.g. AlSi12CuNiMg, can have tensile strengths as high as 400 MPa, and elongation of around 5 %.

For Peer Review Only

Over the years, many attempts have been made to provide even stronger and more ductile alloys. Inoue and Kimura [1] produced several quasicrystalline strengthened Al-alloys using gas atomisation of the melt, followed by densification with warm extrusion or pressing. Among these alloys, the alloys arising from the Al-Mn-Cu system possessed comparable strength to commercial high-strength aluminium alloys (500-600 MPa), and much better ductility (elongation > 20 %). In these alloys, appropriate properties were achieved by rapid solidification, but not when applying moderate cooling rates. To date several new Al-casting alloys strengthened by the quasicrystalline phase have been developed. However, in most cases, besides the quasicrystalline phase several additional intermetallic phases have also been found, adversely affecting ductility [2-4]. In addition, most of these alloys possessed rather high liquidus temperatures exceeding 800 °C, which may be inconvenient for aluminium foundries.

Recently an $Al_{94}Mn_2Cu_2Be_2$ alloy was developed possessing mainly i-phase in the Al-rich solid solution matrix (α-Al). This i-phase was formed at moderate cooling rates typical for conventional die-casting, the liquidus temperature of the alloy being below 700 °C [5]. Previous investigations have shown that (1) Mn is a transition element enabling the formation of metastable quasicrystals [6], Be reduces critical cooling rate for quasicrystal formation [3], while Cu can stabilize i-phase [7], enable strengthening by precipitation hardening, and reduce the liquidus temperature [8]. However, in order to exploit the potential of the Al-Mn-Cu-Be alloy system to the greatest extent, it is necessary to determine the effect of alloying elements and processing conditions on the microstructural evolution and mechanical properties, in a more systematic way.

For Peer Review Only

2 Materials and methods

Four alloys were investigated during this study, and their chemical compositions are given in Table 1. The content of Al in each alloy was above 92 at. % in order to provide large fraction of though aluminium solid solution. Be-content was varied with the aim to obtain information whether quasicrystalline phase may form even at very small amounts of beryllium. Different Mn-contents were selected to influence the fractions of intermetallic phases, and consequently the final mechanical properties. The alloys were prepared from pure Al 99.9, and AlBe5.5, AlMn20 and AlCu50 master alloys using vacuum-induction melting. Thereafter, they were die-cast into a cylindrical copper die with a diameter of 50 mm (approximate cooling rate was few K s^{-1}), and into a smaller copper die with dimensions 100 mm × 10 mm × 1 mm (approximate cooling rate was 1000 K s^{-1}). The samples were investigated using a SEM (Sirion 400 NC, FEI) equipped with EDS (Inca 350, Oxford Instruments), XRD (synchrotron radiation, λ = 0.99598 nm, Sincrotrone Elettra, Trieste, Italy), and Tof SIMS (Time-of-Flight Secondary Ion-Mass Spectroscopy, Cameca TOF-IV). The samples for transmission electron microscopy TEM (Titan 80-300, FEI) were prepared using focussed ion beam technique (Helios Nanolab, FEI). The indentation hardness tests were carried out on a Fisherscope H100C testing machine (Fisher Technology). The loading and unloading times were 10 seconds each. The maximum load applied was 1 N. The results were evaluated using EN-standard [9]. Differential scanning calorimetry (DSC) was performed in an STA 449 Jupiter between 100 °C and 1100 °C, with heating and cooling rates of 20 K min^{-1} in a nitrogen atmosphere.

For Peer Review Only

3 Results

3.1 Microstructural characterization

3.1.1 Slow-cooling

Figure 1 shows backscattered electron micrographs of all alloys after casting into a larger die. Each alloy contained several phases. The phases labelled in the micrographs were identified using *Z*-contrast analysis [10], XRD (Fig. 2), EDS-results and Tof SIMS (Fig. 3). The phases were rather coarse with sizes up to a few hundred microns. The microstructure of the ternary alloy $Al_{94}Mn_3Cu_3$ was composed of Al-rich solid solution (α-Al), and four intermetallics: Al_4Mn, Al_6Mn, τ_1 ($Al_{29}Mn_6Cu_4$) and θ-Al_2Cu. Al_4Mn was mainly surrounded by Al_6Mn, while Al_6Mn was surrounded by τ_1. θ-Al_2Cu was present at the sites where solidification had terminated. Such distribution of phases strongly indicates that the solidification followed a sequence of reactions in the ternary Al-Mn-Cu phase diagram. However, the binary peritectic reaction (L + Al_4Mn → Al_6Mn) and the ternary transition reaction (L + Al_6Mn → τ_1 + α-Al) did not move on to completion due to non-equilibrium solidification conditions. Thus, in this alloy, Al_4Mn and Al_6Mn remained in the microstructure at room temperature besides the equilibrium phases: τ_1, θ-Al_2Cu and α-Al. The peaks of the equilibrium phases dominated in the XRD-spectra, while the peaks of the minor phases Al_4Mn and Al_6Mn were often superimposed by other peaks (Fig. 2). It should be noted that Al_4Mn, τ_1, and Al_6Mn possess rather large unit cells [8]. Consequently, they can be more easily identified at lower angles, while at higher angles their peaks overlap with other peaks. The lattice parameters of the present phases were: a = 0.4029 ± 0.0010 nm for FCC α-Al; a = 0.6049 ± 0.0015 nm and c = 0.4857 ± 0.0007 nm for tetragonal Θ-Al_2Cu (0.3 % different in comparison to PDF 89-1981); a = 2.4113 ± 0.0090 nm, b = 0.7724 ± 0.0040

For Peer Review Only

nm and c = 1.2506 ± 0.0030 nm for orthogonal τ_1(; and a = 0.7523 ± 0.0040 nm, b = 0.6496 ± 0.0050, c = 0.8831 ± 0.0045 for orthogonal Al_6Mn, whereas it was not possible to reliably determine the lattice parameters of hexagonal Al_4Mn due to its very small volume fraction. The lattice parameters of Θ-Al_2Cu, τ_1 and Al_6Mn was almost the same as in the corresponding PDF-files. The lattice parameter of α-Al was approximately 1.5 % smaller than that of pure Al, presumably due to smaller atomic radii of substitutional Cu and Mn atoms.

The addition of Be brought some important microstructural changes:

- Al_6Mn was absent in the quaternary alloys.
- The fraction of Al_4Mn became larger, especially in the alloy $Al_{92.4}Mn_{4.4}Cu_{1.6}Be_{1.6}$ containing the highest Mn-content. The lattice parameters of hexagonal Al_4Mn were: a = 1.9958 ± 0.0170 and c = 2.4711 nm ± 0080 nm, which was almost identical to the published values.
- The fraction of τ_1 became smaller, and its lattice parameters were impossible to determine reliably. It was predominantly present in the form of a thin layer around the Al_4Mn-particles, as well in the regions where solidification had ended.
- A Be-rich phase occurred that presumably formed during the terminal stages of solidification.

In most phases, the analysis of Be normally presents a problem because a phase must contain a very high Be-content to be detected using EDS. However, Be-rich phases can be recognized in the backscattered electron micrographs based on their *Z*-contrast. These phases are much darker than would be expected according to their chemical composition obtained using EDS because when using EDS, only the contents of Al, Mn

For Peer Review Only

and Cu could be determined [10]. It was discovered that in all Be-rich particles, the sums of Cu- and Mn-content as atomic percentages were equal to the Al-contents. This suggested that the possible Be-phase was $Be_4Al(Mn,Cu)$, and not a Raynor phase $Al_{15}Mn_3Be_2$ [11]. This was also confirmed by XRD-results, which revealed that the lattice parameter of $Be_4Al(Mn,Cu)$ was close to that of pure cubic Be_4AlMn (a = 0.6110 ± 0.0010 nm). Thus Cu can partly substitute Mn in Be_4AlMn, which was also found for Ni [12]. On the other hand, Fleury et al. [13] found that Si can replace both Mn and Al in Be_4AlMn. Be_4AlMn can also represent a very suitable heterogeneous nucleation site for the i-phase [13, 14]. In the investigated alloys $Be_4Al(Mn,Cu)$ emerged during the terminal stages of solidification, whereas it appeared at the beginning of solidification in $Al_{94}Mn_2Cu_2Be_2$ [5].

Fig. 3 shows Tof SIMS mapping of Al-, Cu-, Be-, and Mn-ions. It is clear that Be is not only in the Be-rich phase $Be_4Al(Mn,Cu)$, but also in τ_1, Al_4Mn and θ-Al_2Cu. However, the content of Be must be rather small, in the order of a few atomic percentages. There is almost no Be in the Al-rich solid solution, which is consistent with its very low maximum solubility in Al [15].

Fig. 4 shows DSC-cooling curves. All curves clearly show three peaks, despite the fact, that even during solidification of the ternary alloy, many more processes should take place [8]. However, other peaks cannot be seen due to overlapping with the main peaks. The DSC-heating curves were qualitatively the same, indicating the appearance of the same reactions during heating and cooling. It is important that the liquidus temperature stayed below 740 °C, even for the alloy $Al_{92.4}Mn_{4.4}Cu_{1.6}Be_{1.6}$ containing the highest cumulative amount of Be and Mn. This is still appropriate for the practical applications of these alloys in Al-foundries. The previously investigated alloy $Al_{94}Mn_2Be_2Cu_2$ [5],

For Peer Review Only

possessed the liquidus temperature below 700 °C, and the alloy $Al_{95.4}Mn_{1.8}Cu_{1.5}Be_{1.3}$ with somewhat lower amounts of alloying elements had even as low liquidus temperature as 655 °C. Based on the comparison of DSC-traces with the backscattered electron micrographs in Fig. 1, it is possible to predict the main processes taking place on the appearance of peaks. Peaks denoted with 1 indicate the beginning of primary solidification when Al_4Mn starts to form ($L \rightarrow Al_4Mn$), peaks denoted by 2 indicate the formation of α-Al (perhaps via the transition reaction $L + Al_4Mn \rightarrow \alpha\text{-Al} + \tau_1$), whilst peaks 3 indicate the occurrence of the last stages of solidification, when θ-Al_2Cu and $Be_4Al(Mn,Cu)$ formed. In all four-component alloys, the starting temperatures of peaks 3 are similar to the temperature of the ternary eutectic reaction in the Al-Mn-Cu system: $L \rightarrow \alpha\text{-Al} + \theta\text{-}Al_2Cu + \tau_1$. In four component alloys, microstructural investigation indicates that even four phases ($\alpha\text{-Al} + \tau_1 + \theta\text{-}Al_2Cu + Be_4Al(Mn,Cu)$) were present in larger interdendritic spaces (Fig. 1c).

3.1.2 Moderate-cooling

Fig. 5 shows backscattered electron micrographs of the investigated alloys after casting in a small copper die, and Fig. 6 their corresponding X-ray diffraction patterns. There are profound differences in the microstructures and phase compositions compared to the samples cooled at the lower cooling rates (Figs. 1 and 2). In all alloys, except in the ternary, large intermetallic phases were eliminated. In the $Al_{94}Mn_3Cu_3$ alloy, primary Al_4Mn particles were present in the microstructure, however their sizes were within the range of only 5–10 μm, only occasionally Al_6Mn was found. Small fractions of τ_1 and θ-Al_2Cu were merely found in the interdendritic spaces. Be also had an important effect on microstructural evolution at higher cooling rates. The icosahedral quasicrystalline phase formed in all Be-bearing alloys, in contrast to the ternary $Al_{94}Mn_3Cu_3$ alloy. This

For Peer Review Only

can either be a part of a two-phase heterogeneous structure, which can be called binary eutectic, consisting of an α-Al and lamellar i-phase (Fig. 5a-c) or as a primary i-phase in the form of a petal-like particles or well developed dendrite (Fig. 5d).

Primary i-phase dendrites were very frequent in $Al_{92.4}Mn_{4.4}Cu_{1.6}Be_{1.6}$ having the highest Mn-content, whereas they were encountered only occasionally in $Al_{96.5}Mn_{1.3}Cu_{1.6}Be_{0.6}$ and $Al_{95.4}Mn_{1.8}Cu_{1.5}Be_{1.3}$. The fraction of the binary eutectic increased along with the higher Be- and Mn-contents. θ-Al_2Cu can be found in the interdendritic spaces of all alloys, and its peaks are rather pronounced in XRD-spectra (Fig. 6). In addition, another phase, presumably Al_4Mn, envelopes the (α-Al + i-phase) cells in $Al_{92.4}Mn_{4.4}Cu_{1.6}Be_{1.6}$ (Fig. 5d), and its peaks can be found in the XRD-trace (Fig. 6). The peaks of i-phase were rather broad, and often shifted from their ideal positions, indicating the presence of large phason strains. The presence of i-phase was further confirmed using TEM. Fig. 7a shows few branches of the eutectic i-phase. Its selected area diffraction pattern taken along a fivefold direction revealed clearly its quasiperiodic nature (Fig. 7b). Twofold diffraction pattern allowed us to determine its quasilattice constant that was found to be 0,46 nm, which is the same as in the binary Al-Mn alloy. The lattice parameters of other phases present in moderately cooled samples did not differ much from the lattice parameters of the same phases in the slowly cooled samples.

Be was concentrated in the i-phase (Fig. 8) because no other Be-rich phase; e.g. $Be_4Al(Mn,Cu)$ was present. This means, that the i-phase can dissolve considerable amounts of Be, which makes it more stable. This was suggested by Song et al. [3], and experimentally confirmed by using AES for the i-phase in the Al-Mn-Be [16] and Al-Mn-Be-Si [13] alloys.

For Peer Review Only

3.1.3 Heating and annealing

The samples cast into the smaller die were exposed to uniform heating of 20 K min^{-1} up to 600 °C, which is slightly above the solidus temperatures of all alloys. The resulting DSC-traces are depicted in Fig. 9. The ternary alloy exhibited a larger exothermic peak starting at approximate 500 °C (denoted by 2). As the beryllium content increases, this peak grows smaller, and in the alloy $Al_{92.4}Mn_{4.4}Cu_{1.6}Be_{1.6}$ it can hardly be observed. On the other hand, a peak denoted with 1 started to appear by the addition of Be. These results suggest that the initial microstructure becomes unstable above 400 °C for four-component alloys, whereas decomposition of microstructure begins above 500 °C in the ternary alloy.

Figs. 10 and 11 clearly point to some variations in microstructures and phase compositions compared to the as-cast condition. The most striking effect is the appearance of τ_1-peaks in all alloys, and its lattice parameters were apparently identical to those published in Ref. 8. Phase τ_1 almost completely replaces Al_4Mn in the ternary alloy, and in addition, τ_1-particles precipitate from the solid solution. In the quaternary alloys, most of i-phase was preserved. The shapes of the primary i-phase particles remained almost unchanged, however their surfaces became decorated with τ_1 and $Be_4Al(Mn,Cu)$ particles. The morphology of the eutectic *i*-phase changed completely, namely, branched rods transformed into faceted particles with diameters of 500–1000 nm. A similar transition was found in our previous work [5]. Most of the θ-Al_2Cu phase present in the as-cast condition dissolved to a rather large extent. Needle-like precipitates appeared within α-Al with lengths from 1 to 2 μm and a diameter of 100 nm, their nature has not as yet been investigated in detail, but they might be τ_1.

For Peer Review Only

According to the results of microstructural analysis it is possible to state that the peak on the DSC-curve of the ternary alloy arises from the precipitation of τ_1 in the matrix and transformation of τ_1 into Al_4Mn. In the quaternary alloys, the first peak can be attributed to the precipitation of τ_1 in the α-Al matrix, while the second peak can be assigned to the transformation of i-phase into τ_1 and $Be_4Al(Mn,Cu)$, which definitely occurred at temperatures above 500 °C, since most of the i-phase was preserved during annealing at 500 °C.

3.2 Microstructural evolution upon solidification

The presented results clearly show the strong effects of cooling rate and chemical composition on microstructural evolution in Al-Mn-Cu-(Be) alloys during processing. In the Al-rich corner of the Al-Mn-Cu system, the Mn:Cu ratio has a decisive role in determining equilibrium phases [8], when additions of Cu and Mn exceed their solubility limits in Al. The critical ratio amounts 3:2, when only α-Al and τ_1 are in the equilibrium. When this ratio is higher than 3:2, then the equilibrium phases are α-Al, Al_6Mn and τ_1, whereas when this ratio is smaller than 3:2, then α-Al, θ-Al_2Cu and τ_1 are the equilibrium phases, such in the case of the investigated $Al_{94}Mn_3Cu_3$ alloy.

Even during slow-cooling, all five phases are present near the Al-rich corner of the ternary Al-Cu-Mn system formed upon solidification. This is unsurprising because solidification is an inherently non-equilibrium process, linked with spatial and temporal varying temperature and compositional fields. The non-equilibrium phases Al_4Mn and Al_6Mn were formed during the initial stages of solidification and were not consumed completely by the subsequent peritectic and transition reactions [8]. Nevertheless, at least local solidification conditions did not strongly deviate from the equilibrium conditions. On the other hand, a faster cooling rate strongly influenced the nucleation

For Peer Review Only

and growth of phases. It completely suppressed the formation of Al_6Mn and partly τ_1, but strongly enhanced the formation and growth of Al_4Mn. It should be remembered that the equilibrium phase in the Al-Mn phase diagram, μ-Al_4Mn [17], and other strongly related Al-Mn intermetallic phases [14, 18], possess very large unit cells, and icosahedral-cluster substructures. Thus, the cluster substructure existing in the supercooled melt [19], which is achieved by higher cooling rates, can facilitate the formation of such phases.

Additions of Be to Al-Mn-Cu alloys promote the formation of Al_4Mn even at slow cooling rates, whereas the icosahedral phase forms at higher-cooling rates only. Both phases are characterized by the icosahedral cluster substructure. This strongly suggests that the Be-addition strengthens the icosahedral local order in the melt, as previously proposed by Song et al. [3]. Upon slow cooling, only a low supercooling of the melt is attained. Under such conditions, icosahedral clusters can arrange themselves in a periodic way and Al_4Mn forms. However, at higher supercooling the growth rate increases and clusters can only arrange themselves in a quasiperiodic way.

Be-additions completely prevent the formation of Al_6Mn on solidification. This can be based on kinetic or perhaps even thermodynamic reasons. In the latter case, the relative stability of Al_4Mn relative to Al_6Mn is increased. This can enlarge the primary solidification field for Al_4Mn compared to that of Al_6Mn. Be addition and the increased cooling rate also suppress the formation of τ_1. This can be explained by the fact that τ_1 is a quasicrystalline approximant for a decagonal quasicrystal [20] and therefore, the preferred icosahedral order in the melt may not be convenient for the formation of τ_1.

For Peer Review Only

3.3 Microstructural evolution on heating and annealing

During annealing, the system wants to attain the equilibrium condition. In the case of the ternary alloy, it is α-Al + τ_1 + θ-Al_2Cu. The results suggest that it occurs in two steps: (1) partial dissolution of θ-Al_2Cu and precipitation of τ_1-phase from the solid solution, and (2) transformation of primary Al_4Mn to τ_1. It seems that the latter process takes place in-situ, resulting in the same shape of τ_1 as Al_4Mn. Precipitates τ_1, formed during the first step, obviously provide sufficient hardening effect to prevent any softening during annealing. The same effect was observed during the extruding of Al-Mn-Cu-Zr alloy [22].

The equilibrium phases in Al-Mn-Cu-Be are strongly affected by the ratio Mn : Cu = 3 : 2. For the alloys $Al_{96.5}Mn_{1.3}Cu_{1.6}Be_{0.6}$ and $Al_{95.4}Mn_{1.8}Cu_{1.5}Be_{1.3}$ (Mn : Cu < 3 : 2) the expected equilibrium phases are τ_1 + θ-Al_2Cu + α-Al + $Be_4Al(Mn,Cu)$, and for $Al_{92.4}Mn_{4.4}Cu_{1.6}Be_{1.6}$ (Mn : Cu > 3 : 2): τ_1 + Al_4Mn + α-Al + $Be_4Al(Mn,Cu)$. The $Be_4Al(Mn,Cu)$ appears because the Be-contents exceed the cumulative solubility of Be in α-Al, Al_4Mn, τ_1 and θ-Al_2Cu. It is also a two step process, precipitation of τ_1 in α-Al, and transformation of i-phase to τ_1 + $Be_4Al(Mn,Cu)$. It seems that the latter process is rather sluggish, since most of i-phase remained in the microstructure after 1 h annealing at 500 °C. However, increasing the temperature above 500 °C triggered this transformation.

3.4 Microindentation and hardness measurements

Table 2 summarizes the results of microindentation and hardness measurements. It is evident that the lowest mechanical properties were exhibited by the slowly cooled samples. This can be attributed to the very coarse microstructure. Such microstructure

For Peer Review Only

also caused rather large scattering of the results in these samples in comparison to other two conditions. Nevertheless, all alloys were considerably strengthened compared to pure aluminium ($HV \approx 0.17$ GPa). In fact, if we take into account that tensile strength is 3.7-times higher than hardness, and then the tensile strength is within the range between 400 MPa and 500 MPa. This is twice higher than the tensile strengths of most Al-Si alloys, and comparable to the strengths of the strongest Al-cast alloys. Strengthening is probably achieved by combination of precipitation and dispersion hardening. All phases are namely much harder than the Al-rich matrix [22]. The reduced elastic modulus is comparable to that of pure aluminium; it is slightly increased only in the alloy $Al_{92.4}Mn_{4.4}Cu_{1.6}Be_{1.6}$. The low values for the fraction of elastic energy, η_{IT}, also indicate the possibility of strong plastic deformation. Annealing at 500 °C caused a softening of quaternary alloys for about 25 %, but it did not affect the hardness of the ternary alloys. This can be attributed to the strengthening effect of τ_1 [21].

It was discovered that it is possible to obtain much higher strengths of quasicrystal-strengthened cast Al-alloys [2, 4], however, these alloys had reduced ductility, and also rather high liquidus temperatures.

The optimal additions of alloying elements are required, in order to achieve appropriate strength after solidification and to enable further strengthening with precipitation hardening. Firstly, approximately 0.5–1 at. % Be is necessary for promoting the formation of an i-phase during solidification. Secondly, for achieving sufficient volume fractions of hardening phases, i.e. formation of i-phase and suppression of other intermetallic phases during solidification, and τ_1 after annealing, the Mn-content should be 3–3.5 at.% Mn. Thirdly, for facilitating appropriate precipitation hardening the approximate Cu-content should for 2 at.% exceed the fraction of Cu bonded to τ_1 and

For Peer Review Only

$Be_4Al(Mn,Cu)$: 0.66 × at. % Mn + 0.25 × at. % Be; that is (≈4–4.5 at.% Cu). Such a composition will provide sufficient volume fraction of tough α-Al and a liquidus temperature in the range of 700 °C, which is still acceptable for aluminium high-pressure die-casting.

4 Conclusions

The results of this investigation can lead us to the following conclusions:

(1) Both the cooling rate and chemical compositions of the alloys in Al-rich Al-Mn-Cu-(Be) alloys have profound effects on microstructural evolution.

(2) Faster cooling rate (≈1000 K s^{-1}) suppresses the formation of Al_6Mn and τ_1, and promotes the formation Al_4Mn. However, it cannot trigger the formation of an i-phase in the ternary $Al_{94}Mn_3Cu_3$ alloy.

(3) Be-additions prevent the formation of Al_6Mn even at slow cooling rates, and facilitate the formation of an i-phase at higher cooling rates. A considerable effect can be obtained with rather low additions (≈ 0.5 at.% Be)

(4) Heating and annealing of the alloys lead to the formation of stable τ_1-phase and $Be_4Al(Mn,Cu)$, partial or complete dissolution of θ-Al_2Cu, and to the decomposition of metastable Al_4Mn and i-phase. A quasicrystalline i-phase remained in the samples annealed for 1 hour at 500 °C, yet the shapes of primary i-phase particles changed, as well as eutectic rodlike i-phase.

(5) Solidification with a moderate cooling rate (≈1000 K s^{-1}) caused considerable strengthening, which was reduced by annealing by up to 25 % in quaternary alloys, while in the ternary alloy hardness remained almost the same.

For Peer Review Only

Acknowledgements. We would like to thank Dr. Tonica Bončina and Dr. Peter Panjan for their kind assistance during indentation measurements. Rok Šulek (UM FS) is acknowledged for the vacuum melting and casting of alloys. We acknowledge Elettra, Sincrotrone Trieste, and the European Commission for reimbursement under EU contract RII3-CT-2004-506008 (IA-SFS), proposal 20090314. This work was also supported by the European Commission – Research Infrastructure Action under the FP6 "European Integrated Activity of Excellence and Networking for Nano and Micro-Electronics Analysis". Project Number "026134 (RI3) ANNA". This work was partly financed from the research programme P2 - 0120, of the Slovenian Ministry of Higher Education and Science.

5 References

[1] A. Inoue, H. Kimura, High-strength Al-based alloys consisting mainly of nanoscale quasicrystalline or amorphous particles, in: Synthesis and Properties of Mechanically Alloyed and Nanocrystalline Materials, Pts 1 and 2 - Ismanam-96, 1997, p. 873.

[2] F. Schurack, J. Eckert, L. Schultz, Acta Mater., 49 (2001) p. 1351.

[3] G.S. Song, E. Fleury, S.H. Kim, W.T. Kim, D.H. Kim, J. Mater. Res., 17 (2002) p. 1671.

[4] I.H. Jun, J.M. Kim, K.T. Kim, W.J. Jung, Mater. Sci. Eng. A-Struct. Mater. Prop. Microstruct. Process., 449 (2007) p. 979.

[5] F. Zupanic, T. Boncina, N. Rozman, I. Anzel, W. Grogger, C. Gspan, F. Hofer, B. Markoli, Z. Kristall., 223 (2008) p. 735.

[6] D. Shechtman, I. Blech, D. Gratias, J.W. Cahn, Physical Review Letters, 53 (1984) p. 1951.

[7] J.Q. Guo, A.P. Tsai, J. Mater. Res., 16 (2001) p. 3038.

[8] H. L. Lukas, Aluminum - Copper – Manganese, in Ternary alloys: a comprehensive compendium of evaluated constitutional data and phase diagrams, G. Petzow and G. Effenberg, eds., Weinheim; Basel (Switzerland); Cambridge; New York, NY, VCH Verlagsgesellschaft mbH., p. 567.

[9] EN ISO 14577-1:2002 Metallic materials - Instrumented indentation test for hardness and materials parameters - Part 1: Test method, (2002).

For Peer Review Only

[10] F. Zupanic, Mater. Charact., 61 (2010) p. 1335.

[11] G.V. Raynor, C.R. Faulkner, J.D. Noden, A.R. Harding, Acta Metall., 1 (1953) p. 629.

[12] Aluminum-Beryllium-Manganese System, in Aluminum alloys, Structure and Properties, L.F. Mondolfo, ed., London, Boston, Sydney, Wellington, Durban, Toronto, Butterworths-London, 1976, p. 447.

[13] E. Fleury, H.J. Chang, D.H. Kim, Philos. Mag., 86 (2006) p. 349.

[14] T. Boncina, B. Markoli, F. Zupanic, J. Microsc.-Oxf., 233 (2009) p. 364.

[15] J. Murray, D. Kahan, Al-Be (Aluminum-Beryllium), in: *Binary Alloy Phase Diagrams*, T. Massalski, ed., ASM International, 1990, p. 125.

[16] F. Zupanic, T. Boncina, A. Krizman, W. Grogger, C. Gspan, B. Markoli, S. Spaic, J. Alloy. Compd., 452 (2008) p. 343-347.

[17] C.B. Shoemaker, D.A. Keszler, D.P. Shoemaker, Acta Crystallogr. Sect. B-Struct. Commun., 45 (1989) p. 13.

[18] S.H. Kim, G.S. Song, E. Fleury, K. Chattopadhyay, W.T. Kim, D.H. Kim, Phil. Mag. A, 82 (2002) p. 1495.

[19] M.W. Chen, I. Dutta, T. Zhang, A. Inoue, T. Sakurai, Appl. Phys. Lett., 79 (2001) p. 42.

[20] X.Z. Li, K.H. Kuo, Philos. Mag. B-Phys. Condens. Matter Stat. Mech. Electron. Opt. Magn. Prop., 66 (1992) p. 117.

[21] H. Adachi, W. Itaka, T. Aida, K. Osamura, M. Imaoka, J. Kusui, Trans. Indian Inst. Met., 62 (2009) p. 163.

[22] T. Boncina, M. Cekada, B. Markoli, F. Zupanic, J. Alloy. Compd., 505 (2010) p. 486.

For Peer Review Only

Table captions

Table 1: Chemical composition of the alloys cast into a 1-mm copper die, determined using inductively coupled plasma – atomic emission spectroscopy

	$Al_{94}Mn_3Cu_3$	$Al_{96.5}Mn_{1.3}Cu_{1.6}Be_{0.6}$	$Al_{95.4}Mn_{1.8}Cu_{1.5}Be_{1.3}$	$Al_{92.4}Mn_{4.4}Cu_{1.6}Be_{1.6}$
	at. %	at. %	at.	at.%
Mn	2.86	1.25	1.82	4.44
Cu	3.12	1.58	1.53	1.57
Be	0	0.62	1.24	1.58
Al	94.02	96.55	95.41	92.41
Mn/Cu	0.92	0.79	1.19	2.82
Be + Mn	2.85	1.87	3.06	6.02

For Peer Review Only

Table 2: Microindentation properties (load 1 N) and Vickers hardness of alloys cast into a small copper-die in the as-cast (s – slow cooling, m – moderate cooling) conditions and in the annealed (a) condition. *HM* – Martens hardness, HV_{IT} – Vickers indentation hardness, E_r – reduced modulus, η_{IT} – fraction of the elastic energy, *HV* 1 – Vickers hardness (load 10 N)

		$Al_{94}Mn_3Cu_3$	$Al_{96.5}Mn_{1.3}Cu_{1.6}Be_{0.6}$	$Al_{95.4}Mn_{1.8}Cu_{1.5}Be_{1.3}$	$Al_{92.4}Mn_{4.4}Cu_{1.6}Be_{1.6}$
HM / GPa	s	1.10	0.92	0.99	0.87
	m	1.18	1.08	1.20	1.43
	a	1.17	0.97	0.87	1.20
HV_{IT} / GPa	s	0.99	0.80	0.88	73.63
	m	1.10	0.98	1.12	1.37
	a	1.11	0.89	0.80	1.11
E_r / GPa	s	74.65	75.68	83.68	79.58
	m	75.99	79.05	73.20	81.48
	a	73.56	71.33	69.39	80.09
η_{IT} / %	s	10.38	8.39	10.3	9.37
	m	13.06	11.39	13.6	15.26
	a	13.62	11.49	10.5	13.17
HV 1 / GPa	s	0.98	0.95	0.99	1.01
	m	1.13	1.10	1.17	1.60
	a	1.16	0.98	0.88	1.15

For Peer Review Only

Figure captions

Figure 1: Backscattered electron micrographs after vacuum induction melting and casting into a cylindrical 50-mm die: a) $Al_{94}Mn_3Cu_3$ b) $Al_{96.5}Mn_{1.3}Cu_{1.6}Be_{0.6}$, c) $Al_{95.4}Mn_{1.8}Cu_{1.5}Be_{1.3}$ and d) $Al_{92.4}Mn_{4.4}Cu_{1.6}Be_{1.6}$. Note that no Al_6Mn formed in the quaternary alloys, while the Be-rich phase $Be_4Al(Mn,Cu)$ appeared in the interdendritic regions.

Figure 2: 2D-XRD after VIM for a) $Al_{94}Mn_3Cu_3$ b) $Al_{96.5}Mn_{1.3}Cu_{1.6}Be_{0.6}$, c) $Al_{95.4}Mn_{1.8}Cu_{1.5}Be_{1.3}$ and d) $Al_{92.4}Mn_{4.4}Cu_{1.6}Be_{1.6}$. Note that the heights of τ_1- and θ-Al_2Cu-peaks considerably reduced in the quaternary alloys, but the heights of Al_4Mn-peaks increased. The peaks of $Be_4Al(Mn,Cu)$ are hardly seen due to its very small volume fraction.

Figure 3: Tof SIMS mapping of Al-, Cu-, Be- and Mn-secondary ions in $Al_{95.4}Mn_{1.8}Cu_{1.5}Be_{1.3}$ after slow cooling (few K s^{-1}). Note that Be is present in all phases, yet its content is negligible in the α-Al.

Figure 4: DSC-traces obtained at a cooling rate of 20 K min^{-1} for $Al_{94}Mn_3Cu_3$, $Al_{96.5}Mn_{1.3}Cu_{1.6}Be_{0.6}$, $Al_{95.4}Mn_{1.8}Cu_{1.5}Be_{1.3}$ and $Al_{92.4}Mn_{4.4}Cu_{1.6}Be_{1.6}$. Peak 1: primary crystallization of Al_4Mn, peak 2: formation of α-Al, and peak 3: terminal stage of solidification.

Figure 5: Microstructures of alloys after casting into a 1-mm die for a) $Al_{94}Mn_3Cu_3$ b) $Al_{96.5}Mn_{1.3}Cu_{1.6}Be_{0.6}$, c) $Al_{95.4}Mn_{1.8}Cu_{1.5}Be_{1.3}$ and d) $Al_{92.4}Mn_{4.4}Cu_{1.6}Be_{1.6}$. Approximate cooling rate was 1000 K s^{-1}. In the ternary alloy, primary Al_4Mn dominates, with very small fractions of τ_1 and θ-Al_2Cu in interdendritic spaces. In the quaternary alloy i-phase formed, but no τ_1, $Be_4Al(Mn,Cu)$, Al_4Mn and Al_6Mn. Only in alloy $Al_{92.4}Mn_{4.4}Cu_{1.6}Be_{1.6}$ was an additional phase (presumably Al_4Mn) formed around the (i-phase + α-Al) eutectic cells. In all alloys, θ-Al_2Cu formed during terminal stages of solidification.

Figure 6: XRD-traces for $Al_{94}Mn_3Cu_3$, $Al_{96.5}Mn_{1.3}Cu_{1.6}Be_{0.6}$, $Al_{95.4}Mn_{1.8}Cu_{1.5}Be_{1.3}$ and d) $Al_{92.4}Mn_{4.4}Cu_{1.6}Be_{1.6}$ after casting into a 1-mm copper die. Peaks of θ-Al_2Cu, Al_4Mn and α-Al are observed in the ternary alloy. In quaternary alloys in addition to θ-Al_2Cu, rather wide peaks belonging to i-phase appeared. Only in the $Al_{92.4}Mn_{4.4}Cu_{1.6}Be_{1.6}$ alloy, also additional peaks presumably belonging to Al_4Mn can be seen.

Figure 7: Icosahedral quasicrystalline phase as a part of binary i-phase and α-Al eutectic. a) Bright-field transmission electron micrograph, and b) the corresponding selected area diffraction pattern taken along a fivefold axis.

Figure 8: Tof SIMS mapping of Al-, Cu-, Be- and Mn-secondary ions in $Al_{95.4}Mn_{1.8}Cu_{1.5}Be_{1.3}$ after solidification in a small Cu-die (cooling rate ≈ 1000 K s^{-1}). Note that Be is present in both the primary and eutectic i-phase.

Figure 9: Heating curves for a) $Al_{94}Mn_3Cu_3$ b) $Al_{96.5}Mn_{1.3}Cu_{1.6}Be_{0.6}$, c) $Al_{95.4}Mn_{1.8}Cu_{1.5}Be_{1.3}$ and d) $Al_{92.4}Mn_{4.4}Cu_{1.6}Be_{1.6}$

For Peer Review Only

Figure 10: Backscattered electron micrographs of the alloys a) $Al_{94}Mn_3Cu_3$ b) $Al_{96.5}Mn_{1.3}Cu_{1.6}Be_{0.6}$, c) $Al_{95.4}Mn_{1.8}Cu_{1.5}Be_{1.3}$ and d) $Al_{92.4}Mn_{4.4}Cu_{1.6}Be_{1.6}$ annealing at 500 °C for 1 hour. In alloy $Al_{94}Mn_3Cu_3$, τ_1 almost completely replaced Al_4Mn. Additional τ_1 precipitates formed in the α-Al matrix. θ-Al_2Cu coagulated in rounded particles. In the quaternary alloys, rods of eutectic i-phase turned into particles, almost whole θ-Al_2Cu dissolved in the matrix, whilst in the matrix a high fraction of precipitates formed. Primary i-phase remained, however its surface became covered with τ_1 and $Be_4Al(Mn,Cu)$.

Figure 11: XRD-traces of alloys a) $Al_{94}Mn_3Cu_3$ b) $Al_{96.5}Mn_{1.3}Cu_{1.6}Be_{0.6}$, c) $Al_{95.4}Mn_{1.8}Cu_{1.5}Be_{1.3}$ and d) $Al_{92.4}Mn_{4.4}Cu_{1.6}Be_{1.6}$ annealed at 500 °C for 1 h. In all alloys the fractions of τ_1 increased considerably, whereas the fractions of θ-Al_2Cu decreased. In the ternary alloy the Al_4Mn-peaks disappeared almost completely, whilst they were considerably reduced in the alloy $Al_{92.4}Mn_{4.4}Cu_{1.6}Be_{1.6}$. In all quaternary alloys i-phase remained, however its peaks start to overlap with those of τ_1.

For Peer Review Only

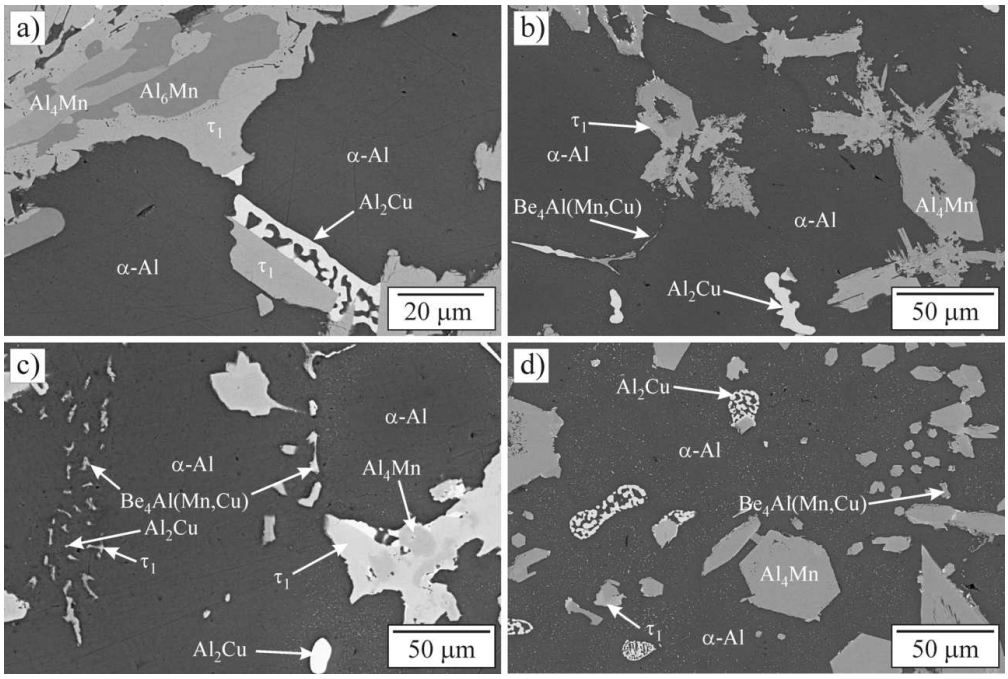

Microstructure after slow cooling
a) Al-Mn-Cu, b-d)Al-Mn-Cu-Be alloys
108x72mm (300 x 300 DPI)

For Review Only

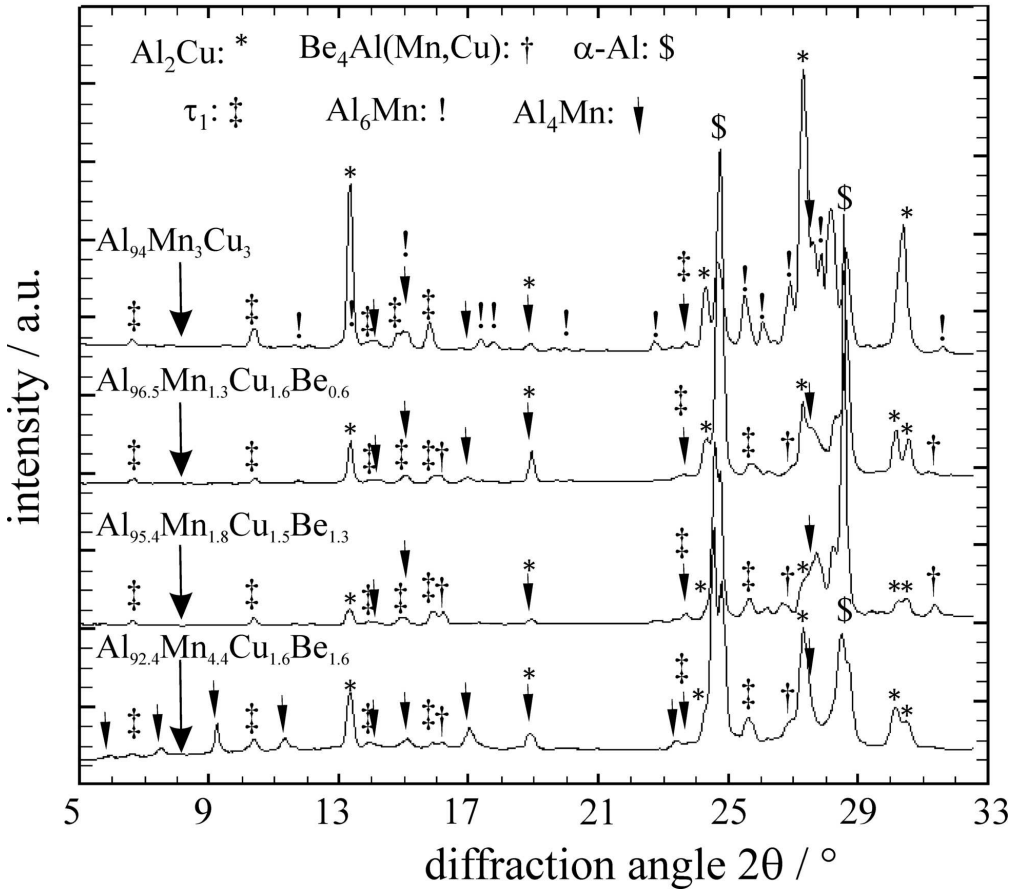

X-ray diffraction traces after slow cooling
82x73mm (600 x 600 DPI)

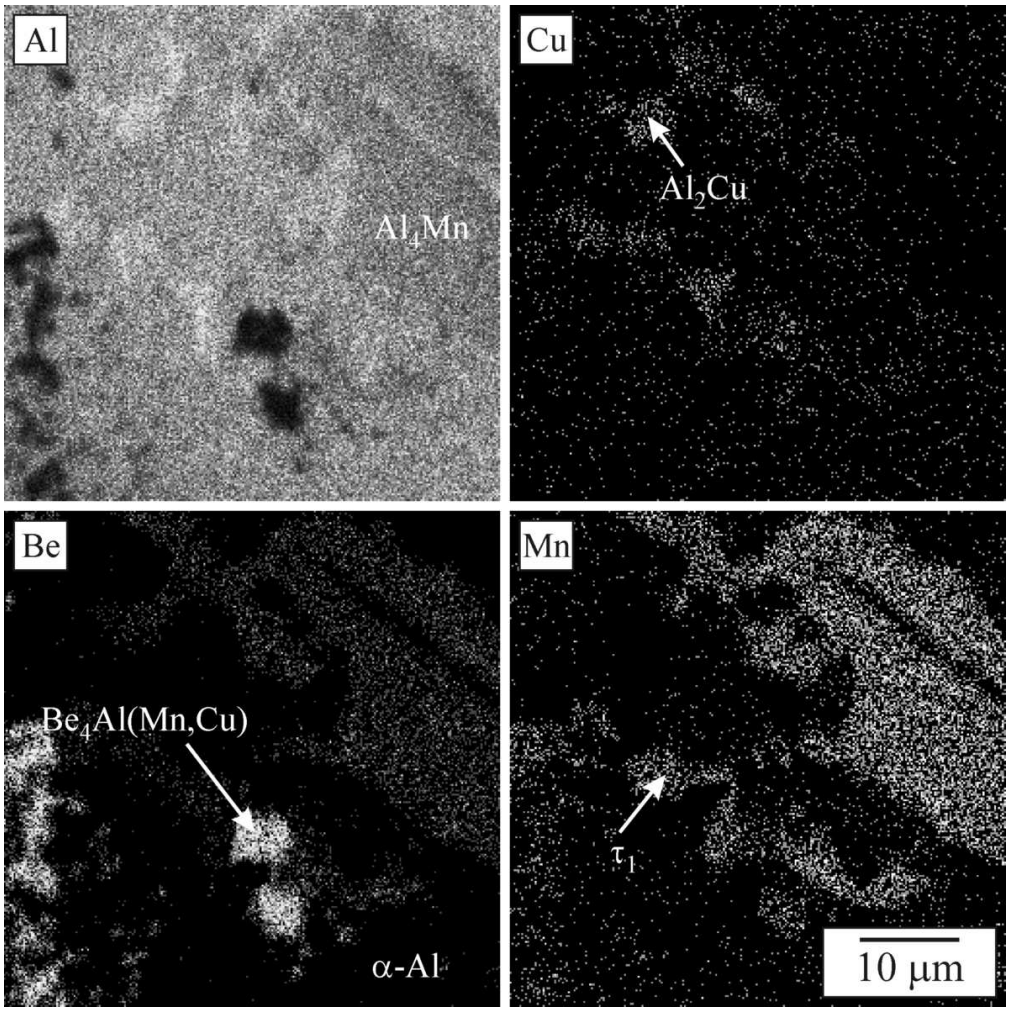

Tof-SIMS mapping of a quaternary alloy after slow cooling
100x100mm (300 x 300 DPI)

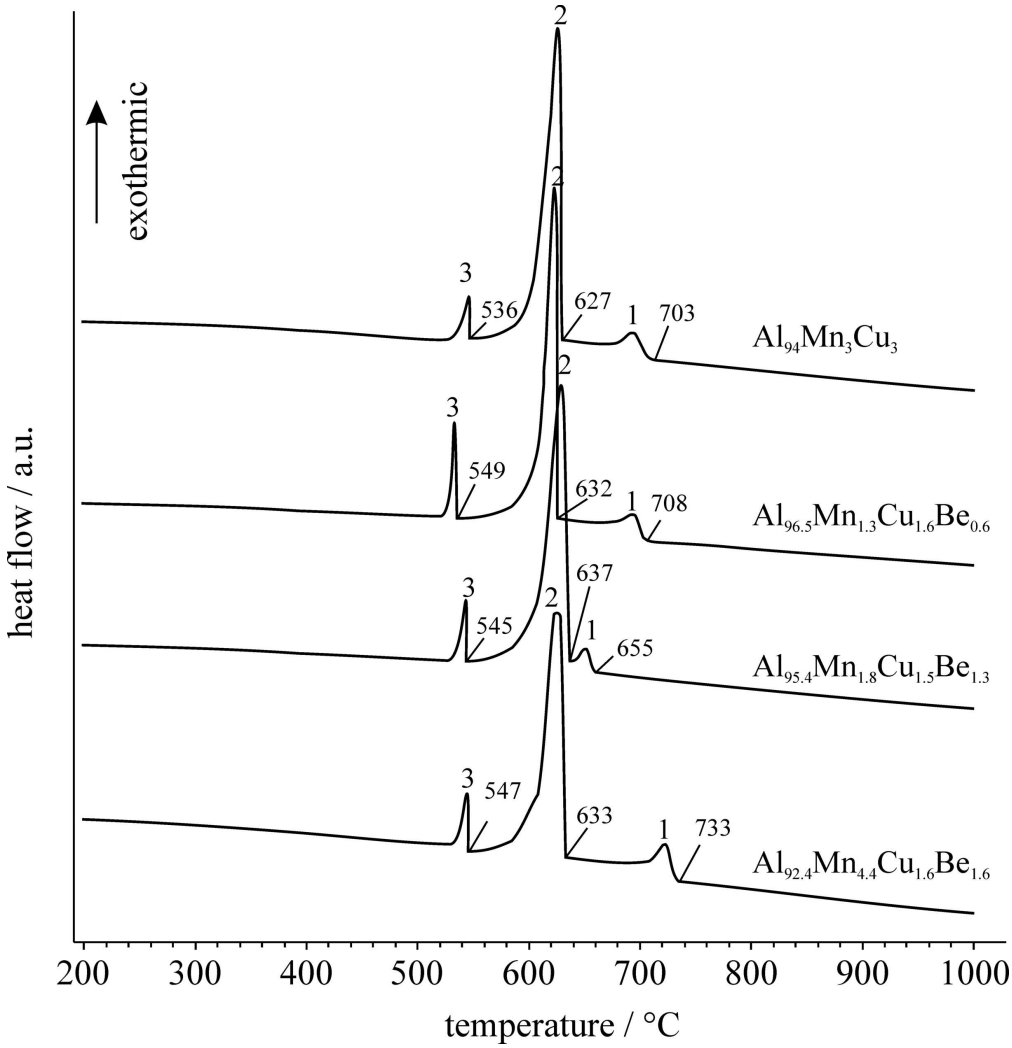

DSC cooling curves for Al-Mn-Cu and Al-Mn-Cu-Be alloys
102x106mm (600 x 600 DPI)

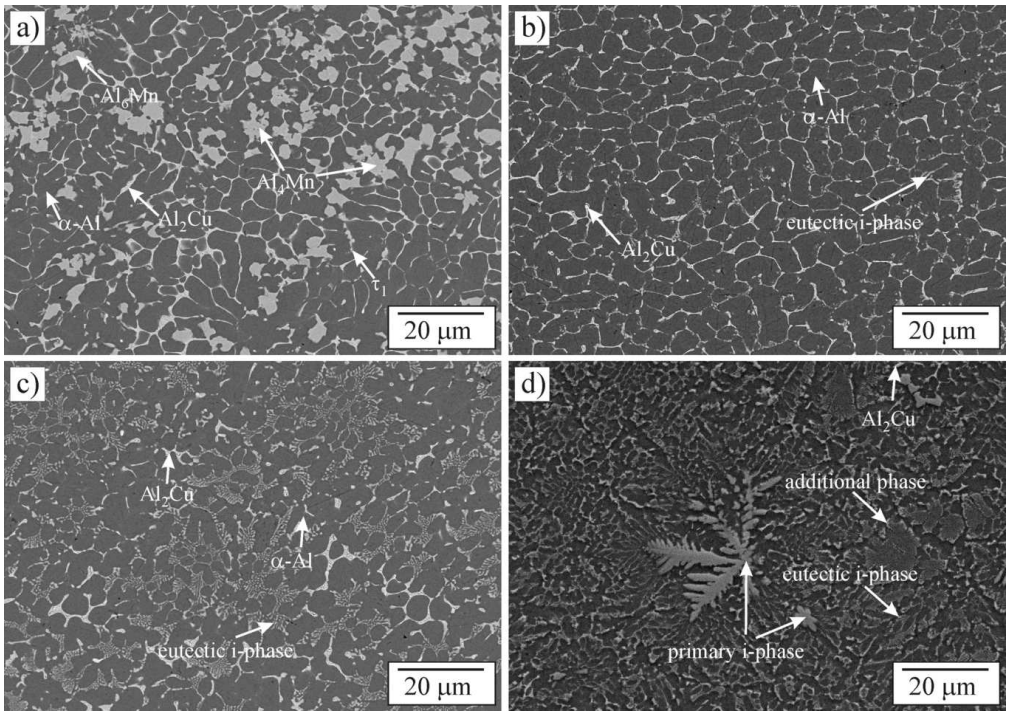

Microstructure of Al-Mn-Be and Al-Mn-Be-Cu alloys after moderate cooling
114x80mm (300 x 300 DPI)

View Only

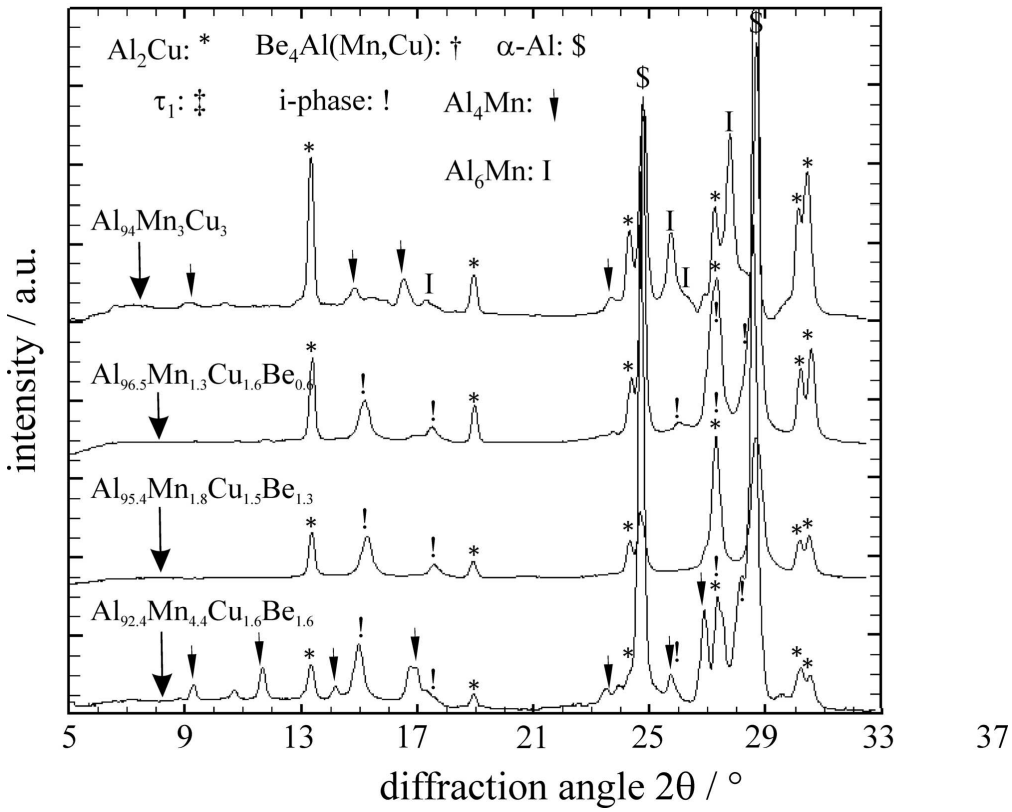

XRD traces for Al-Mn-Cu and Al-Mn-Cu-Be alloy after moderate cooling
84x68mm (600 x 600 DPI)

ew Only

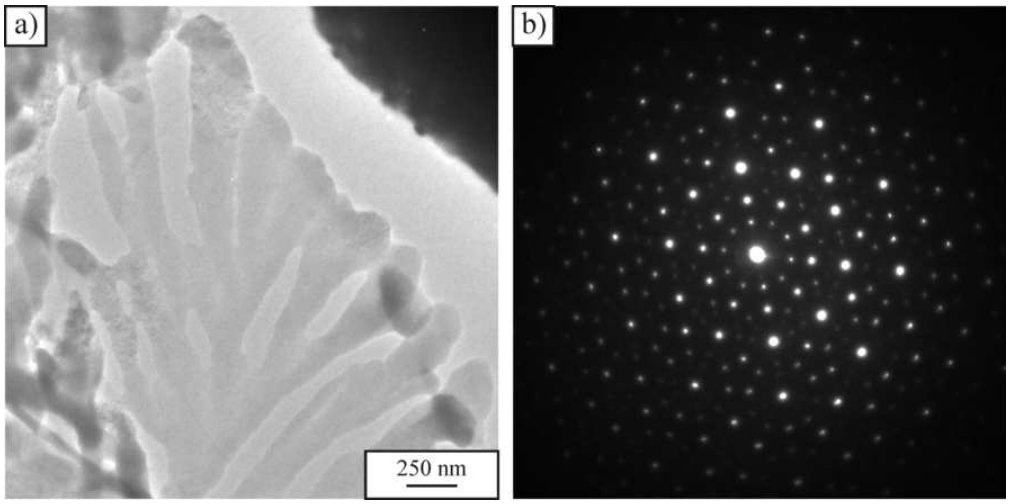

TEM micrograph of eutectic icosahedral phase and its fivefold diffration pattern
75x37mm (300 x 300 DPI)

For Review Only

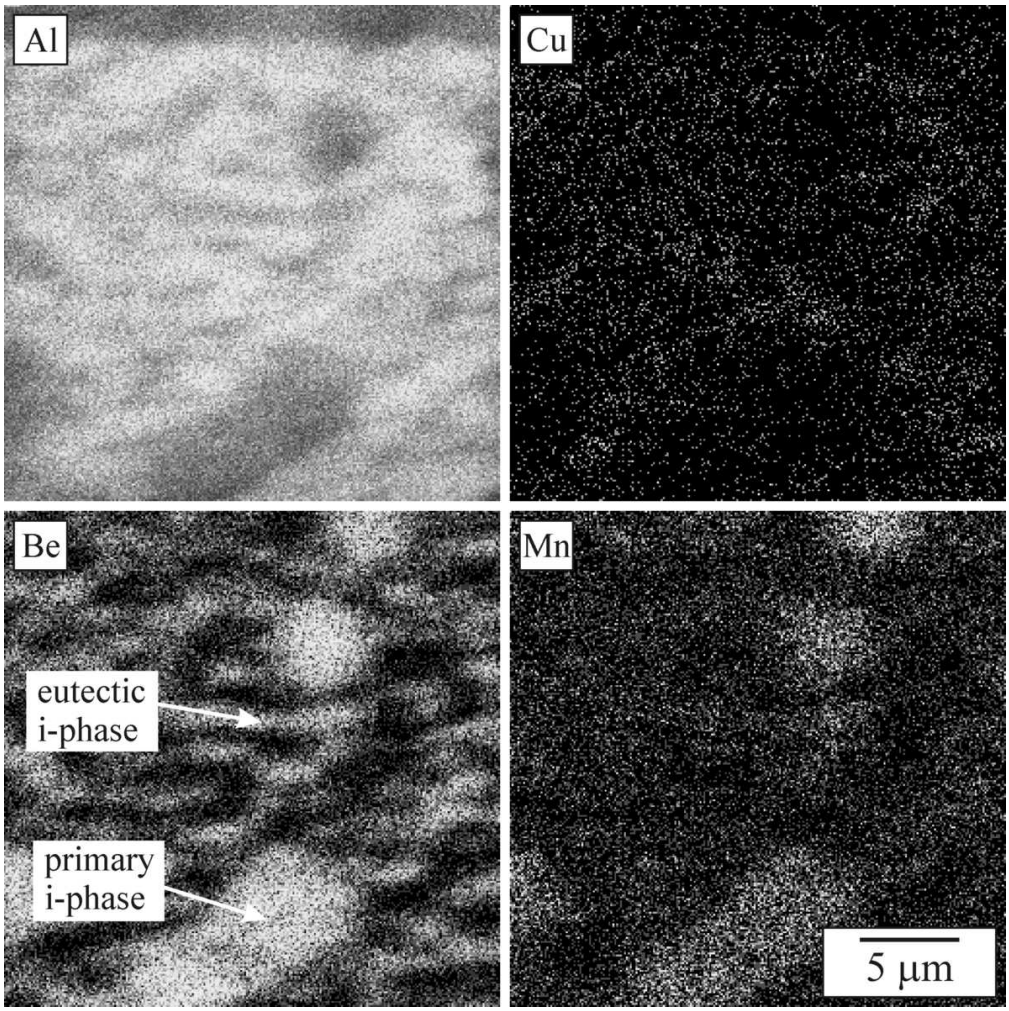

Tof SIMS mapping of the icosahedral phase in Al-Mn-Cu-Be alloy after moderate cooling
100x100mm (300 x 300 DPI)

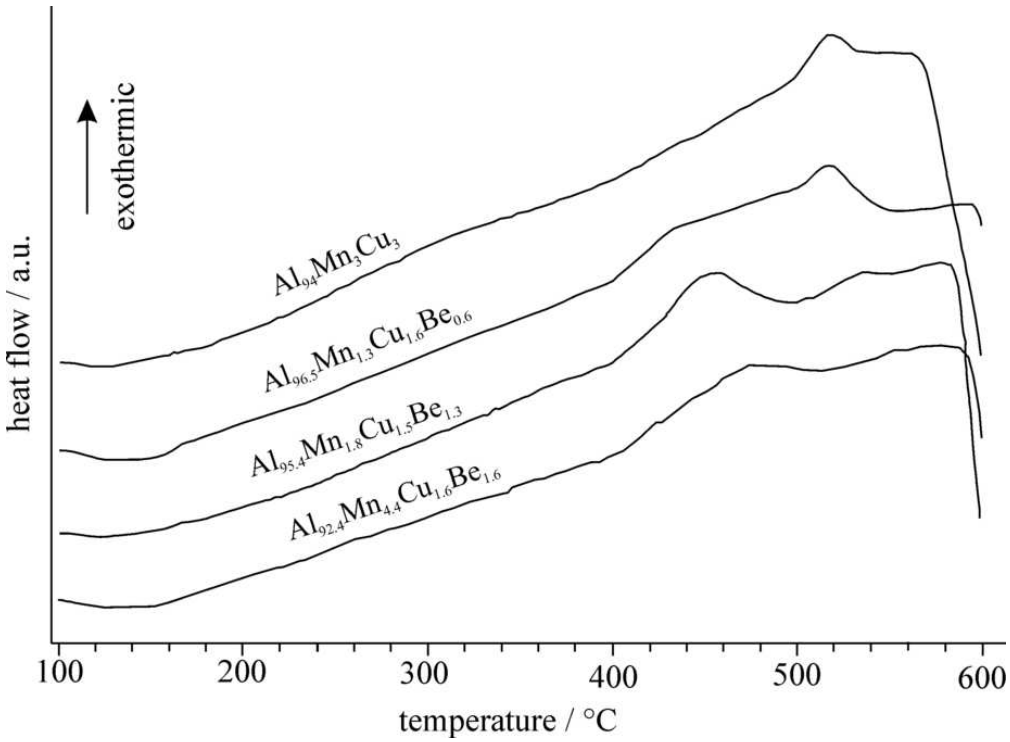

DSC heating curves, initial contion, moderately cooled samples
77x57mm (300 x 300 DPI)

View Only

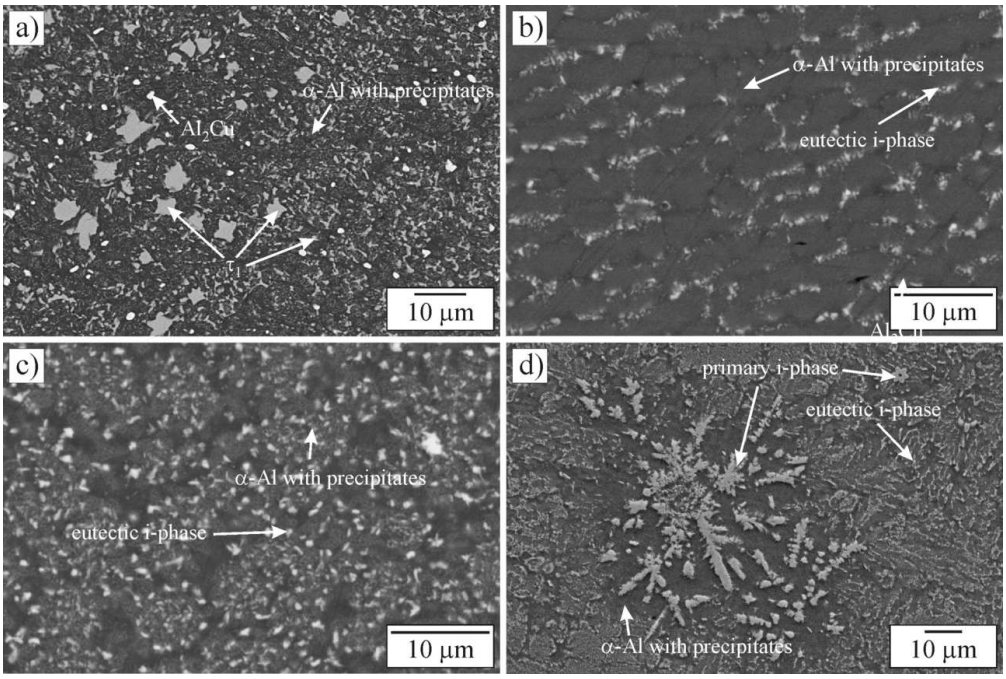

Microstructures after annealing moderately cooled samples, 500 deg C, 1 h
108x72mm (300 x 300 DPI)

Review Only

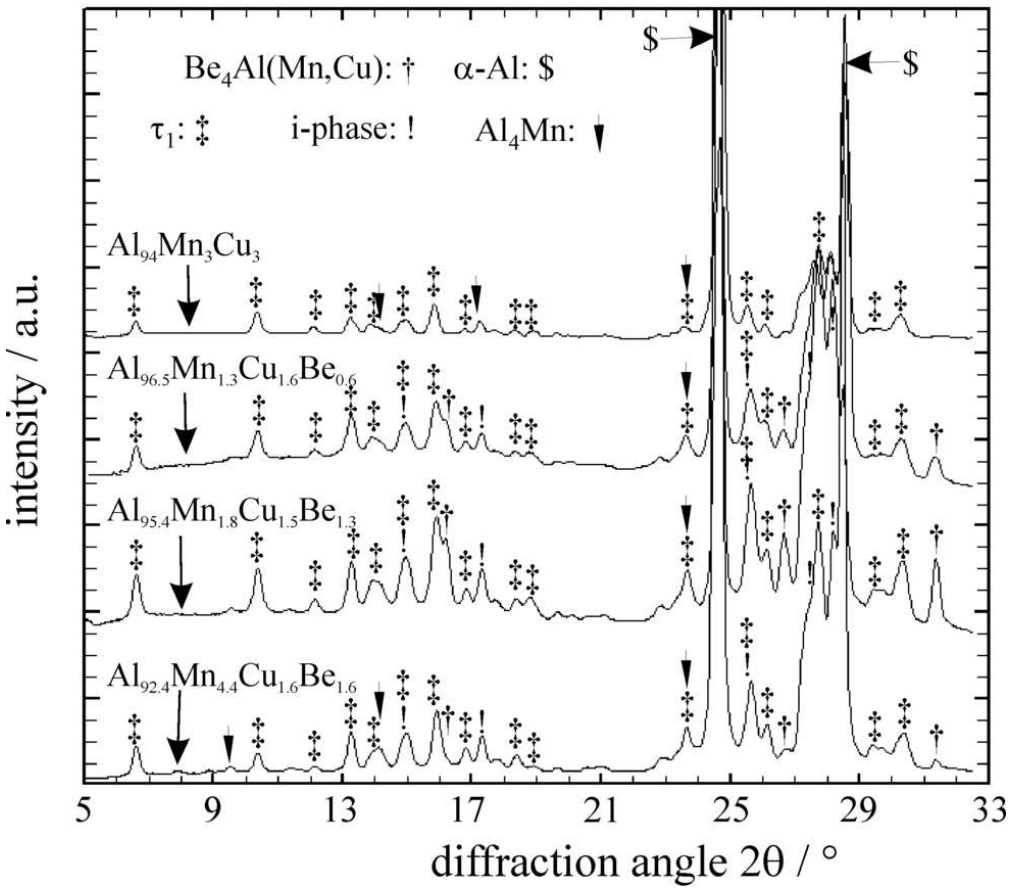

XRD traces after annealing for 1 h at 500 deg C
82x73mm (300 x 300 DPI)

	$Al_{94}Mn_3Cu_3$	$Al_{96.5}Mn_{1.3}Cu_{1.6}Be_{0.6}$	$Al_{95.4}Mn_{1.8}Cu_{1.5}Be_{1.3}$	$Al_{92.4}Mn_{4.4}Cu_{1.6}Be_{1.6}$
	at. %	at. %	at.	at.%
Mn	2.86	1.25	1.82	4.44
Cu	3.12	1.58	1.53	1.57
Be	0	0.62	1.24	1.58
Al	94.02	96.55	95.41	92.41
Mn/Cu	0.92	0.79	1.19	2.82
Be + Mn	2.85	1.87	3.06	6.02

For Peer Review Only

		$Al_{94}Mn_3Cu_3$	$Al_{96.5}Mn_{1.3}Cu_{1.6}Be_{0.6}$	$Al_{95.4}Mn_{1.8}Cu_{1.5}Be_{1.3}$	$Al_{92.4}Mn_{4.4}Cu_{1.6}Be_{1.6}$
HM / GPa	s	1.10	0.92	0.99	0.87
	c	1.18	1.08	1.20	1.43
	a	1.17	0.97	0.87	1.20
HV_{IT} / GPa	s	0.99	0.80	0.88	73.63
	c	1.10	0.98	1.12	1.37
	a	1.11	0.89	0.80	1.11
E_r / GPa	s	74.65	75.68	83.68	79.58
	c	75.99	79.05	73.20	81.48
	a	73.56	71.33	69.39	80.09
η_{IT} / %	s	10.38	8.39	10.3	9.37
	c	13.06	11.39	13.6	15.26
	a	13.62	11.49	10.5	13.17
HV 1 / GPa	s	0.98	0.95	0.99	1.01
	c	1.13	1.10	1.17	1.60
	a	1.16	0.98	0.88	1.15

For Peer Review Only